NEOPLASIA
www.neoplasia.com

Volume 20 Number 8 August 2018 pp. 848–856 848

# Off-Target and Tumor-Specific Accumulation of Monocytes, Macrophages and Myeloid-Derived Suppressor Cells after Systemic Injection

**Francis Combes[*], Séan Mc Cafferty[*], Evelyne Meyer[†,‡] and Niek N. Sanders[*,‡]**

[*]Laboratory of Gene Therapy, Department of Nutrition, Genetics and Ethology, Faculty of Veterinary Medicine, Ghent University, Heidestraat 19, B-9820 Merelbeke, Belgium; [†]Department of Pharmacology, Toxicology and Biochemistry, Faculty of Veterinary Medicine, Ghent University, Salisburylaan 133, 9820 Merelbeke, Belgium; [‡]Cancer Research Institute Ghent (CRIG), Ghent, Belgium

## Abstract

Solid tumors frequently coexist with a degree of local chronic inflammation. Recruited myeloid cells can therefore be considered as interesting vehicles for tumor-targeted delivery of therapeutic agents. Using *in vivo* imaging, the short-term accumulation of systemically injected monocytes, macrophages and myeloid-derived suppressor cells (MDSCs) was compared in mice bearing fat pad mammary carcinomas. Monocytes and macrophages demonstrated almost identical *in vivo* and *ex vivo* distribution patterns with maximal tumor-associated accumulation seen 48 hours after injection that remained stable over the 4-day follow-up period. However, a substantial accumulation of both cell types was also seen in the liver, spleen and lungs albeit decreasing over time in all three locations. The MDSCs exhibited a similar distribution pattern as the monocytes and macrophages, but demonstrated a better relative on-target fraction over time. Overall, our findings highlight off-target cell accumulation as a major obstacle in the use of myeloid cells as vehicles for therapeutic tumor-targeted agents and indicate that their short-term on-target accumulation is mainly of nonspecific nature.

*Neoplasia (2018) 20, 848–856*

## Introduction

Many cancers are intrinsically linked to an inflammation reaction associated with the recruitment of white blood cells. Consequently, using myeloid cells as intelligent drug carriers for intricate sensing and conditional release/expression of therapeutic cargoes has been a long-desired goal [1,2]. Ideally, this strategy would concentrate the therapeutic substances at the tumor site avoiding high systemic levels, leading to wider therapeutic windows and hence, better cancer drug safety profiles [3]. Currently, white blood cells are already used as complex vehicles to manipulate a diverse set of biologic processes, as demonstrated by the recent success of CAR T cell therapy [4]. Since the feasibility of engineering immune cells to treat cancer was demonstrated, the focus shifted towards optimization studies. An eminent need for fundamental studies on biodistribution of cell-based therapeutics or cellular drug delivery vehicles emerged [4,5]. In this context, several "tumor-homing" cell types such as tumor-infiltrating lymphocytes (TILs) [3], neutrophils [3,6], mesenchymal stem cells (MSCs) [7] and myeloid-derived suppressor cells (MDSCs) [8] have been investigated. Although the validity of the homing concept was repeatedly demonstrated, most of these migration studies selectively focused on the tumor-specific accumulation. However, information on the accumulation of these cellular vehicles in off-target tissue is limited. As pathologically activated leukocytes of the myeloid lineage such as tumor-associated macrophages (TAMs) [9] and MDSCs [10] are known to accumulate in massive numbers in the tumor microenvironment, the current study evaluated their migration patterns. More specifically, the aim was to assess whether off-target accumulation of these injected myeloid cells forms a barrier in the

Address all correspondence to: Prof. Dr. Niek N. Sanders, Laboratory of Gene Therapy, Department of Nutrition, Genetics and Ethology, Faculty of Veterinary Medicine, Ghent University, Heidestraat 19, B-9820 Merelbeke, Belgium.
E-mail: Niek.Sanders@ugent.be
Received 10 March 2018; Revised 16 June 2018; Accepted 19 June 2018


1476-5586
https://doi.org/10.1016/j.neo.2018.06.005

development of cellular vehicles for the delivery of potentially harmful anticancer agents.

DiR (1,1′-dioctadecyl-3,3,3′,3′-tetramethylindotricarbocyanine iodide) is a non-immunogenic lipophilic carbocyanine near infrared (NIR) dye that is frequently used for *in vivo* migration studies [11-14]. After integration into lipid membranes, DiR becomes a very bright NIR dye that allows non-invasive tracking of labelled cells for several days without interfering with their biological function [11,12,15]. In the current study, DiR was used as labelling agent for comparing short-term tumor-tropism of primary monocytes, macrophages and MDSCs. In a murine orthotopic 4T1 mammary adenocarcinoma model, all these myeloid cell types displayed clear visual accumulation in the primary tumors after systemic administration. However, substantial off-target cell sequestration in the liver, spleen and to a minor extent also in the lungs was observed as well. This latter aspect should not be ignored when considering these cellular vehicles for the delivery of cytotoxic agents.

## Materials and Methods

### *Animals*

All procedures in this study were approved by the Ethical Committee of the Faculty of Veterinary Medicine and the Faculty of Bioscience Engineering of Ghent University, Belgium (EC 2015/100). Female BALB/cJRj mice, aged 6-8 weeks, were purchased from Janvier Labs (Paris, France) and housed in a temperature and humidity controlled room while being kept on a 12h:12h reverse light/dark cycle. Ad libitum access to low-fluorescence food (Envigo, Boxmeer, Netherlands, #T.2018.12) and water was provided. Mice were ear marked and randomly assigned to experimental conditions. All manipulations were performed on a heated platform and under general anesthesia using 5% isoflurane (Zoetis, Louvain-la-Neuve, Belgium, #B506) at 4 L/min oxygen for induction and 1.5-2% isoflurane at 0.5-1 L/min oxygen for maintenance.

### *Tumor Model*

Luciferase-positive 4T1 mammary carcinoma cells were cultured in complete medium consisting out of DMEM/F12 (Gibco, #21041-025) supplemented with 10% heat inactivated FBS (Biowest, #S181H-500) and 1% penicillin/streptomycin (Gibco, #15070-063). After at least 3 passages, cells were trypsinized and washed twice in Dulbecco's Phosphate-Buffered Saline (DPBS, (Gibco, #14190-144). Subsequently, $1\times10^5$ cells in 100 µl DPBS, were injected in the 4$^{th}$ right fat pad using a 29G insulin syringe (Terumo, Leuven, Belgium, #BS05M2913). Tumor growth was verified by administering 200 µl D-luciferin (15 mg/ml DPBS) (Goldbio, St-Louis (MO), USA, #LUCK-1G) subcutaneously followed by bioluminescence imaging after 10 min with an IVIS Lumina II system (PerkinElmer). Cell migration experiments were initiated 10 days post tumor inoculation. At this timepoint, tumors reached an average diameter of 4.73 mm (range 3.77 mm to 6.18 mm). This average tumor diameter was obtained by measuring both perpendicular diameters twice and then averaging the total of 4 measurements.

### *Primary Cells*

Bone marrow cells were isolated from female BALB/cJRj mice according to the method described by Amend et al. (2016) [16]. Mice were induced with isoflurane and sacrificed via cervical dislocation. Next, femurs and tibias were dissected, sterilized 10 seconds in 70% Disinfectol (Chem-lab NV, Zedelgem, Belgium, #CL00.0112.2500) and rinsed in sterile DPBS before snapping the bones in half and transferring these to punctured 0.5 ml Eppendorf tubes that were placed in empty 1.5 ml EP tubes. After centrifugation for 15 seconds at 10,000xg, recovered pellets were resuspended 40 seconds in ACK RBC lysis buffer (Gibco, #A10492-01) and neutralized by transferring the solution to 10 ml DPBS. Finally, these cells were centrifuged for 5 min at 400xg and resuspended in complete medium.

Monocyte-derived cells were obtained by seeding RBC-depleted bone marrow cells ($4x10^6$ cells/4 ml per dish) in complete medium supplemented with 20 ng/ml M-CSF (VWR, Leuven, Belgium, #21-8983-U010). To drive monocyte-derived cells towards differentiation in macrophages—hereafter referred to as 'macrophages'—cells were cultured for 7 days in 9 cm untreated petri dish (allowing easier detachment) [17] (VWR, Leuven, Belgium, #734-2311). Macrophages were collected via mechanical dissociation with cell scrapers (VWR, Leuven, Belgium, #734-2602) after washing in 10 mM EDTA (Gibco, #15575-038) in DPBS and adding complete medium. Monocyte-derived cells intended to maintain a more immature monocyte status—hereafter referred to as 'monocytes'—were cultured for only 5 days in 6-well ultra-low attachment plates (Sigma-Aldrich, Overijse, Belgium, #CLS3471-24EA) to prevent adherence-induced differentiation [18]. Culture medium was refreshed 3-4 days post-seeding. Only the monocytes in suspension were collected for further experiments. Experiments with 'Antigen-experienced' monocytes were also performed and these were obtained by incubating monocytes with $10^6$ lysed (freeze-thawed twice) 4T1 cells per well 24 h prior to injection.

Primary MDSCs were obtained by harvesting bone marrow cells after RBC lysis from female Balb/cJrj mice bearing a 14-day old 4T1 tumor. *Ex vivo* differentiated MDSCs were obtained by culturing fresh RBC-depleted bone marrow cells from healthy mice (see above) 5 days on 6-well plates in GM-CSF supplemented 4T1-conditioned medium (Navarrabiomed, Pamplona, Spain) complemented with 10% FBS, 1% penicillin/streptomycin and 0.5% gentamycin (ThermoFisher, #15710-049) according to the manufacturer's instructions and as described by Lichtenstein et al. (2014) [19,20].

### *Cell Labelling*

Labelling with DiR (Life, Eugene (OR), USA, #D12731) was performed by adding 5 µM dye (final concentration) to cells suspended in DPBS at a concentration of $1x10^6$/400 µl. After gentle mixing, the cells were incubated for 20 min at 37°C in darkened 15 ml tubes. Subsequently, they were washed twice in at least 4 volumes of cold complete medium before suspending in appropriate downstream buffer (DPBS for injection or staining buffer for flow cytometry).

### *Systemic and Local Injection*

Labelled cells were gently vortexed prior to injection with a 29G insulin syringe. Unless noted otherwise, 100 µl of cells suspended in DPBS were injected in the right orbital plexus of anesthetized mice at a concentration of $10x10^6$/ml [21-24]. Local injection occurred through intratumoral injection of $10^5$ DiR-labelled monocytes (in 50 µl DPBS) into 10-days old 4T1 tumors.

### *Organ Dissociation*

Twenty-four hours after injection of the DiR-labelled cells, mice were euthanized and the liver, spleen, lungs, uterus, kidneys, left 4$^{th}$ mammary gland (tumor-free contralateral control), heart, intestines and primary tumor were collected for each mouse. Subsequently, the

lungs, spleen, liver and primary tumor were dissociated using a gentleMACS system (Miltenyi, Cologne, Germany, #130-093-235), followed by 45 min enzymatic digestion at 37°C in the presence of DNaseI (Worthington, Gestimed Brussels, LS006342, 10 U/ml final concentration) and collagenase IV (Worthington, Gestimed Brussels, LS004186, 100 U/ml final concentration) in DMEM/F12. The resulting single cell suspensions were washed twice in DMEM/F12 (for 5 min at 400xg centrifugation) followed by passing them through a 70 µm cell strainer (Falcon, #352350).

### *Flow Cytometry*

Cells were suspended at $1\times10^6$/ml in 200 µl staining buffer (DPBS + 2%FBS + 2mM EDTA) followed by adding 0.5 µl anti-CD16/32 FcR blocking antibodies (BD, #553142) [25]. After 10 min incubation at 4°C additional fluorescently labelled antibodies against the selected markers were added and the cells were further incubated at 4°C for 15 min. Subsequently, they were washed by adding 1 ml staining buffer per dark 1.5 ml EP tube and centrifuged for 5 min at 400×g. The resulting pellet was resuspended in 200 µl staining buffer. The DNA intercalating dye 7-AAD (Biolegend, #420403) was used to exclude dead cells. A weekly calibrated and validated C6 Accuri (BD) or Cytoflex (Beckman Coulter) flow cytometer was used for acquisition. BD Accuri C6 software (version 1.0.264.21) and Cytexpert 2.0 were used for analysis, respectively. Following selected antibodies were used (all from Biolegend): anti-Ly6C-FITC (#128005), anti-Ly6G-PE (#127607), anti-CD11b (#101211), anti-MHC II-APC (#107613) and anti-CD115 PE (#135505), while anti-F4/80-R-PE was ordered from Biorad (#MCA497PET). Used isotypes (all from Biolegend) were: Rat IgG2c,κ (#400705), Rat IgG2a,κ (#400507) and Rat IgG2b,κ (#400612).

### *In Vivo and Ex Vivo Fluorescence Imaging*

*In vivo* fluorescence imaging of the DIR-labelled cells was performed with an IVIS Lumina II system (PerkinElmer) using the 745/820 nm filter pair. All mice were ventrally shaven from the cervical to the pubis region before imaging. After *in vivo* fluorescence imaging, the accumulation of the labeled cells in the tumor and liver/spleen was quantified using the formula:

$$Accumulation\ factor = \frac{(Organ_{post}/Mam_{post})}{(Organ_{pre}/Mam_{pre})}$$

Where $Organ_{post}$ stands for total fluorescence efficiency (TFE) in the region of interest (ROI) drawn around either the tumor or the liver-and-spleen after injection of the DiR-labelled cells. In most mice, liver and spleen could easily be discriminated, but since spleen mobility can cause spleen and liver to overlap *in vivo*, the fluorescence of these organs was combined into one ROI. $Mam_{post}$ stands for the TFE in the ROI drawn around the naive (tumor-free) mammary gland after injection of DiR-labelled cells. Similarly, $Organ_{pre}$ and $Mam_{pre}$ both represent the TFE in the respective ROI, but before injection of DiR-labelled cells. ROI dimensions were kept constant for all mice. This formula essentially describes the normalized fold change of TFE in the tumor and liver-and-spleen upon injection of the DiR-labelled cells.

*Ex vivo* fluorescence signal of the organs and tumors were quantified using the formula:

$$Fold\ increase = \frac{Organ_{labelled}}{Organ_{unlabelled}}$$

Where $Organ_{labelled}$ stands for the TFE in the ROI drawn around an organ after labelled cells were injected. $Organ_{unlabelled}$ stands for the TFE in the ROI of the same respective organ of another mouse which received an equal number of unlabelled cells. ROI dimensions were kept constant for all mice. This formula essentially describes a fluorescence fold increase value of organs after injection of labelled cells. A fold increase value of 1 means that no change has occurred.

### *Statistics*

Statistics were performed via Prism Graphpad (version 6.01). Unless otherwise specified, two-way ANOVA (using time and condition or time and organ as factors) followed by Tukey's test for multiple comparisons was used in most experiments. A threshold of $p<0.05$ (corrected for multiple comparisons) was used to test for statistical significance. Reported values represent averages ± standard deviation (SD).

## Results

### *In Vivo Migration of Monocytes and Macrophages*

Monocyte-derived macrophages accumulate in massive numbers in the tumor microenvironment [5, 26, 27]. These so-called TAMs are therefore interesting vehicles for tumor targeted delivery of e.g. therapeutic genes. However, the extent to which they specifically accumulate in the tumor after systemic injection remains unclear. The *in vivo* distribution of systemically injected DiR-labelled, bone marrow-derived monocytes (n=5) and macrophages (n=5) was investigated in 4T1 tumors with an average diameter of 4.78± 0.73 mm. Immunophenotypic profiles of these *in vitro* differentiated monocytes and macrophages showed the expected expression of the myeloid marker CD11b (93.2% and 82.4%, respectively) and the monocytic lineage marker F4/80 (62.9% and 72.8%, respectively) in both subsets. Further characterization using monocyte/macrophage maturation markers Ly6C and MHC II demonstrated a less differentiated status of monocytes ($Ly6C^{hi}MHCII^{lo}$) compared to macrophages ($Ly6C^{int}MHCII^{hi}$) (Supplementary Figure 1). DiR-labelled monocytes and macrophages were intravenously injected and their distribution was subsequently monitored over 96 h by *in vivo* fluorescence imaging (Figure 1). Twenty-four hours post injection, both monocytes and macrophages demonstrated a clear visual buildup of fluorescence in all tumors. During the follow-up period, the number of accumulated monocytes and macrophages remained almost constant with average accumulation factors ranging from 1.89—2.35 (±0.19) to 2.19—2.37 (±0.08) for monocytes and macrophages, respectively. No significant differences in tumor accumulation factor between the two cell types were observed ($p\geq0.922$). However, a strong off-target accumulation of these cells was seen in the liver and spleen. The total fluorescence in these off-target organs was significantly higher compared to that in the tumors ($p<0.0004$), with average accumulation factors ranging from 4.09 – 5.18 (±0.55) to 4.76—5.37 (±0.26) for macrophages and monocytes, respectively. Similar to the primary tumor, this combined total *in vivo* fluorescence of the liver-and-spleen did not demonstrate significant differences between monocytes and macrophages ($p\geq0.976$). However, in contrast to the primary tumor, a slight decrease in fluorescence over time was noticed in the liver and spleen. One mouse in the macrophages group was removed from the analysis since its primary tumor spontaneously disappeared at the start of the 4-day follow up

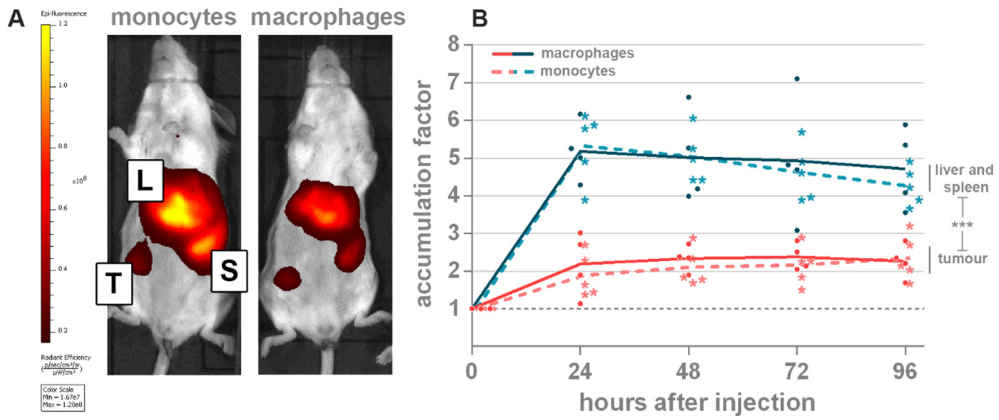


**Figure 1.** In vivo fluorescence signal in tumors (red) or liver and spleen (blue) upon injection of 1x10$^6$ DiR-labelled monocytes (broken line, asterisks) or macrophages (full line, dots). (A) Representative images of two mice 48 h after systemic injection of DiR-labelled monocytes or macrophages. Primary tumors develop in the 4$^{th}$ right abdominal mammary gland. (B) Graph showing the time-dependent DiR fluorescence in the tumor and liver/spleen. Depicted values in the Y-axis represent the in vivo accumulation factor i.e. the corrected fluorescence signal taking into account differences in background fluorescence in the tumor and the liver/spleen (see Materials and methods section). A value of y=1 indicates no increase in fluorescence signal in the tissue compared to the signal before injection of the labelled cells. (*** p<0.0001), n=5. Tumour (T), liver (L), spleen (S).

period. Interestingly, this process was accompanied with a concurrent loss of fluorescence. In Supplementary Figure 2 the complete line-up of all mice before and 48 h after injection of labelled monocytes or macrophages is depicted.

Ninety-six hours after injection, all mice were sacrificed with an average end-stage tumor diameter of 5.98 mm (±0.74). *Ex vivo* fluorescence imaging was performed on the dissected tumors and organs (Figure 2 and Supplementary Figure 3). In line with the *in vivo* fluorescence, a similar tissue accumulation pattern of the monocytes and macrophages was observed. Monocytes demonstrated a 5.53 (±0.69) fold increase at the tumor location, whereas macrophages exhibit a 7.07 (±0.98) fold increase. However, *ex vivo* imaging allowed to identify the liver as the main organ of fluorescence

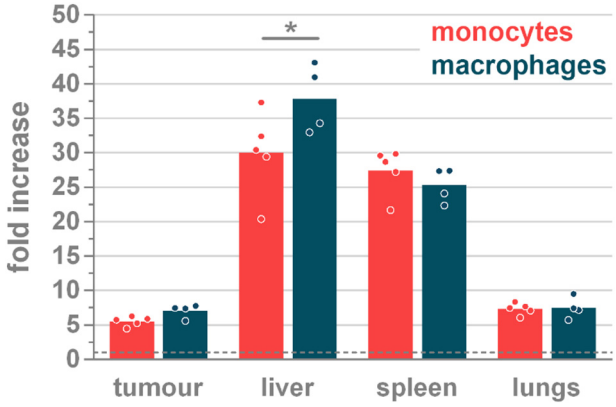


**Figure 2.** Ex vivo fluorescence signal at 96 h in the liver, spleen, lungs and tumor depicted as fold increases over background fluorescence in the respective tissues of mice that were injected with unlabelled cells. Dotted line at y=1 indicates no change in fluorescence. Significant difference between monocytes and macrophages are only detected in the liver (*p=0.0262). Within one cell type, all organs exhibit significantly different fluorescence (p≤0.0262) except for tumor versus lungs (both monocytes and macrophages) and liver versus spleen (monocytes). n=5

accumulation with a 30.00 (±6.16) and 37.85— (±4.95) fold increase over background for monocytes and macrophages, respectively. This was the only significantly different (p<0.0262) organ value for both cell types. In addition to the liver, the spleen was confirmed as the second important organ were the injected cells accumulate with an *ex vivo* fold increase of 27.40 (±3.36) and 25.30 (±2.49) for monocytes and macrophages, respectively. *Ex vivo* imaging further identified the lungs as an important organ of signal retention with fold increases of 7.34 (±0.83) and 7.46 (±1.55) for monocytes and macrophages, respectively, being in the same range as the signals measured in the primary tumor (Figure 2).

We also evaluated tumor migration of unstimulated monocytes versus antigen-experienced monocytes in tumor-bearing mice (Supplementary Figure 4, *A-C*). Until 4 days post injection, antigen-experienced monocytes accumulated significantly more in the liver-and-spleen compared to unstimulated monocytes. No difference in tumor-homing was detected. In addition, we also studied the fate of DiR-labelled monocytes after intratumoral injection in 4T1 tumors. No leakage of DiR fluorescence to the liver and the spleen was detected, indicating high tumoral retention of the injected monocytes (Supplementary Figure 4*D*).

### *In Vivo Assessment of Possible Artefacts*

In a subsequent set of experiments, the extent to which artefacts could have affected our data was studied. Three control experiments were performed. In a first control experiment we determined whether residual free DiR could cause artefacts in the migration pattern. This was done by injecting the supernatant obtained after washing of DiR-labelled macrophages. The second control experiment involved the injection of lysed DiR-labelled macrophages to quantify nonspecific cell debris accumulation. Additionally, we also wondered whether the tumor accumulation of the monocytes/macrophages could be attributed to an active migration process. Therefore, in a third control experiment, the chemotaxis receptors on the macrophages were inactivated by fixing them with paraformaldehyde and injecting these fixed DiR-labelled macrophages. The injected numbers of lysed or fixed macrophages were equal to the number of injected live

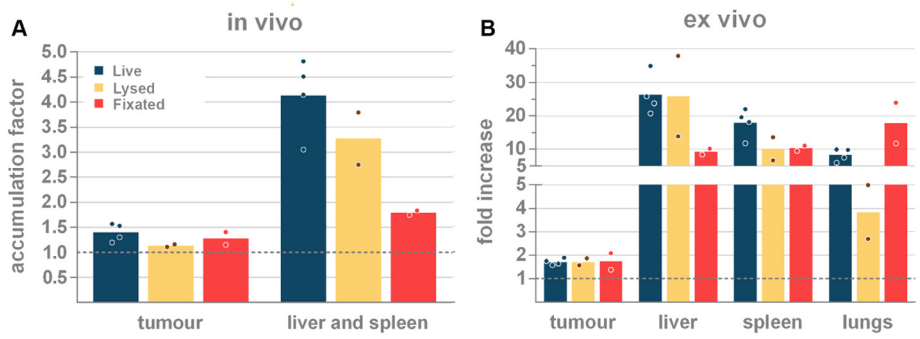


**Figure 3.** (A) Comparison of the in vivo accumulation factor and (B) the ex vivo fold increase in the liver, spleen, lungs and tumor of live, fixed and lysed DiR-labelled macrophages 24 h after their systemic injection. n=4 (live cells), n=2 (controls).

macrophages. To allow a proper comparison, live DiR-labelled macrophages were also repeated in this experiment.

For all three controls, the *in vivo* organ-associated accumulation factor and the *ex vivo* fold increase value was evaluated 24 h after injection (Figure 3). Injection of supernatant did not result in increased fluorescence in the tumor (0.92 ±0.10, p≥0.9113), or in the liver and spleen (1.00 ±0.02, p≥0.9623), demonstrating that the effect of possible residual free dye in the cell suspension can be considered irrelevant (data not shown). Corroborating the data from our previous experiment, live DiR-labelled macrophages are associated with the highest *in vivo* accumulation factor in the tumor (1.40 ±0.18) and in the liver-and-spleen (4.13 ±0.77) (blue bars Figure 3*A*). This was further supported with *ex vivo* fold increase values of 26.31 ±6.11, 17.90 ±4.37 and 1.72 ±0.14 for liver, spleen and tumor, respectively (Blue bars Figure 3*B*). Similar to the live cells (p=0.4168), systemic administration of labelled cell debris (lysed cells) mainly resulted in a high *in vivo* accumulation factor in the liver and spleen (3.27 ±0.74, yellow bars Figure 3*A*). This concordance with live cells was also reflected in the *ex vivo* fold increase values of the liver and the spleen (25.88 ±17.04 and 10.14 ±4.88, respectively; yellow bars Figure 3*B*). As expected, the small cell fragments present in lysed cells caused a much lower accumulation in the lungs (3.85 ±1.62). Compared to live cells, lysed cell debris appeared to be slightly less present at the tumor location *in vivo* (1.14 ±0.03), a measurement that could not be verified *ex vivo* since all conditions led to similar *ex vivo* fold increase values (1.72-1.73 ±0.22) (Figure 3 and Supplementary Figure 5). This equal tumor-associated fluorescence further substantiated the hypothesis of nonspecific accumulation in the tumor. The number of dead cells in our inoculum was determined to vary between 10-15% (Supplementary Table 1). Considering the weak tumor accumulation of cell fragments and the low percentage of dead cells in our inoculum, the effect of dead cells on the tumor accumulation is likely negligible. Still, a small percentage of the off-target accumulation of the immune cells could be attributed to dead cells.

*In vivo*, fixed cells accumulated to a similar extent as live cells in the tumor (1.28 ±0.18, p>0.9999), indicating that tumor-associated accumulation is of passive rather than active nature. In marked contrast to live cells and lysed cells, fixed cells exhibited a much lower *in vivo* accumulation in the liver and spleen (1.79 ±0.06, p=0.0012, red bars Figure 3*A*). The decreased number of fixed cells in the liver (9.32 ±1.23) might be clarified by a marked presence of these cells in the lungs (17.85 ±8.58, p=0.9132, red bars Figure 3*B*). The *ex vivo* fluorescence data shown in Figure 3*B* were further confirmed via flow cytometric analysis on single cell suspensions (Supplementary Figure 5).

### *In Vivo Migration of Myeloid Derived Suppressor Cells*

Myeloid derived suppressor cells (MDSCs) are immature bone marrow-derived myeloid cells that cause immunosuppression and are specifically recruited by solid tumors [8,28]. In particular, mice bearing 4T1 mammary tumors have been demonstrated to possess a remarkable high number of MDSCs in their bone marrow compared to naive mice [29-33]. Therefore, it was studied whether the distribution of *in vitro* differentiated MDSCs [20] or MDSCs obtained from 4T1 tumor-bearing mice showed a different tumor tropism and distribution compared to bone marrow cells of healthy mice after systemic injection (Figure 4). Flow cytometric immunophenotyping prior to injection (Supplementary Figure 6) indicated that bone marrow from 4T1 tumor-bearing donors consisted mainly of myeloid cells (52.8% $CD11b^+$), with a majority of these $CD11b^+$ cells being of the granulocytic MDSC phenotype (22.5% $CD11b^+Ly6G^+Ly6C^{int}$) and to a lesser extent of the monocytic MDSC phenotype (3.6% $CD11b^+Ly6G^-Ly6C^{hi}$). Similarly, the granulocytic phenotype was also overrepresented in the *in vitro* differentiated MDSCs (44.8% versus 8.0% monocytic phenotype within the 90.8% $CD11b^+$ population). In contrast, the bone marrow originating from healthy donors contained a far lower percentage of $CD11b^+$ cells (27.5%) of which only 14.3% were $CD11b^+Ly6G^+Ly6C^{int}$ and 2.4% were $CD11b^+Ly6G^-Ly6C^{hi}$ cells.

At the tumor site, maximal accumulation of the three types of cells remained limited and occurred at later timepoints: the 4T1 tumor-bearing donor derived and *in vitro* differentiated MDSCs exhibited maximal tumor accumulation factors after 48 h (1.46 ±0.22) and 72 h (1.35 ±0.17), respectively; while the signal of healthy donor bone marrow cells continued to increase up until the last timepoint, reaching a tumor accumulation factor of 1.55 (±0.02) (Figure 4*A*).

Similar to the monocytes and macrophages, the highest accumulation of all MDSC types was observed in the liver and spleen at 24 h. This maximal *in vivo* accumulation factor was higher for the *in vitro* differentiated MDSCs (2.80 ±0.62) than for the healthy donor bone marrow cells (2.36 ±0.25) and the 4T1 tumor-bearing donor-derived MDSCs (1.81 ±0.11). At later timepoints, the accumulation factors in the liver and spleen showed a steady decline reaching respective values of 1.88 (±0.26), 1.77 (±0.14) and 1.36 (±0.16) 96 h after injection (Figure 4*B*).

### *Comparing Relative On-Target Migration of Monocytes, Macrophages and MDSCs*

The overall trend in all evaluated myeloid cell types was a time-dependent decrease in off-target accumulation (liver and spleen) and a

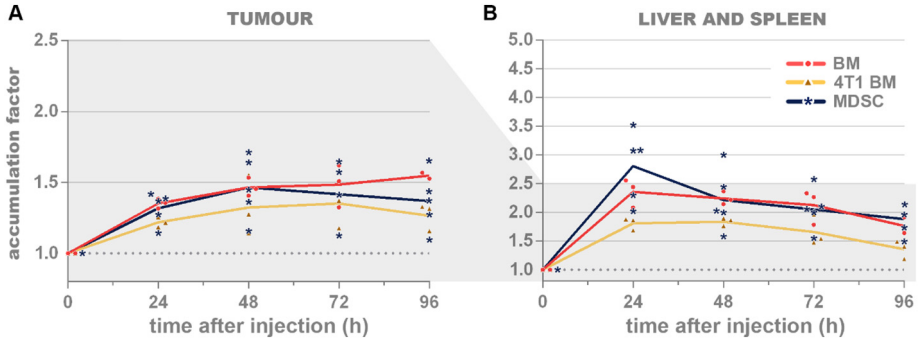


**Figure 4.** In vivo accumulation factors in tumors (A) or liver and spleen (B) upon injection of DiR-labelled bone marrow cells from a healthy donor ('BM', red, dots), MDSCs from a 4T1 tumor-bearing donor ('4T1 BM', yellow, triangles) or in vitro differentiated MDSCs ('MDSC', blue, asterisks). At almost all timepoints, these three types of cells accumulated equally in the tumors and in the liver and/or spleen. Significant differences at the tumor 96 h after injection between BM and 4T1 BM ($p=0.0489$) and at the liver-and-spleen 24 h after injection between MDSCs and 4T1 BM ($p=0.0003$). A value of $y=1$ indicates no increase in signal. MDSCs: myeloid-derived suppressor cells. $n=5$.

generally constant tumor-associated accumulation as shown in Figure 1*B* as well as Figure 4. Figure 5 depicts this relationship as a 'relative on-target' graph where the tumor-associated accumulation, quantified by the *in vivo* accumulation factor, of each cell type is represented as the percentage of the combined signal present in the tumor versus liver and spleen. At the end of the 4-day follow-up period, MDSCs from a 4T1 tumor-bearing donor (48.3% ± 4.4% at 96 h), and bone marrow cells from healthy donor mice (46.8% ±2.1% at 96 h) and *in vitro* differentiated MDSCs (42.1% ± 4.4% at 96 h) exhibited a higher on-target migration than primary monocytes (34.2% ± 3.7% at 96 h) and macrophages (32.8% ± 6.6% at 96 h).

## Discussion

Stem cells, more specifically MSCs, are vigorously pursued to serve as tumor-targeted cellular vehicles due to their immune-privileged and

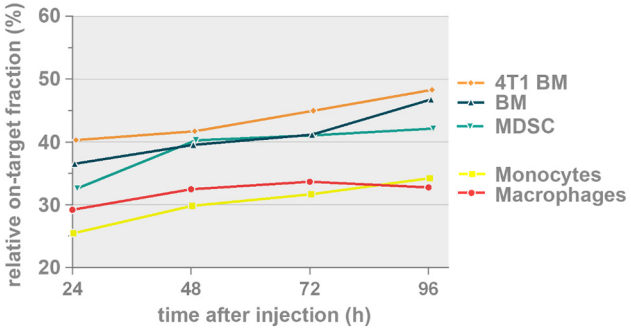


**Figure 5.** Relative percentage of on-target tumor accumulation of the myeloid cells where the tumor-associated accumulation, quantified by the in vivo accumulation factor, of each cell type is represented as the percentage of the combined signal present in the tumor versus liver and spleen (tumor/(tumor + liver and spleen)). Significant differences: monocytes versus MDSCs from 4T1 tumor-bearing donor (at 24 h, 72 h and 96 h; $p<0.05$), monocytes versus bone marrow cells from healthy donor (at 96 h, $p<0.05$), monocytes versus in vitro differentiated MDSCs (at 48 h, $p<0.05$), macrophages versus bone marrow cells from healthy donor (at 96 h, $p<0.05$) and macrophages versus MDSCs from 4T1 tumor-bearing donor (at 96 h, $p<0.01$). MDSCs: myeloid-derived suppressor cells.

-evasive characteristics. These characteristics enable MSCs to be used in allogeneic settings [34]. Moreover, they have been demonstrated to accumulate at the microenvironment of solid tumors. Tempering this promising effect, several groups have observed that only a limited number of injected MSCs reach the tumor and that their main therapeutic properties can be largely attributed to the secretion of soluble factors [7,35,36]. This major caveat led us to explore other cell types which could be used as tumor-targeted vehicles. Particularly myeloid leukocyte subsets have been demonstrated to gather in large numbers in the tumor microenvironment. For example, tumors of 4T1 tumor-bearing mice are characterized by a $CD45^+$ cell population consisting mainly out of myeloid cells (70-90%) and only 2.4–7% $CD3^+$ T cells [37-39]. Most of the myeloid cells in this model have been identified as TAMs (40%) or tumor-associated neutrophils (TANs, 30%) and only a small percentage were dendritic cells (<5%) [39]. Indeed, to successfully establish an immunosuppressive milieu, recruitment of TAMs and MDSCs seems indispensable for solid tumors [40-42]. We therefore reasoned that these myeloid cells are potentially useful as tumor-targeted cellular vehicles. Classically, monocytes are believed to exhibit superior trafficking properties compared to further differentiated macrophages [43,44]. Nevertheless, upon systemic injection of monocytes or macrophages we observed a nearly identical *in vivo* distribution pattern. The normalized accumulation factors demonstrated that both cell types exhibited a clear tumor-associated accumulation 24 h after injection. This accumulation remained stable (or slightly increased) over the 96 h follow-up period. Importantly, both cell types also demonstrated substantial off-target migration to the liver and the spleen. This off-target accumulation in the liver-and-spleen was significantly higher compared to the tumor-associated value and it steadily declined over the 96 h follow-up period. This indicates a continuous clearance of the injected cells from the liver and/or spleen. *Ex vivo* fluorescence imaging at 96 h post injection identified the liver, followed by the spleen, as the two main organs for cell retention. The lungs were identified as a third organ where labelled cells accumulated after systemic injection. An equal accumulation of monocytes and macrophages was observed in almost all organs and no relevant differences in trafficking behavior between monocytes and macrophages could be identified [3,45-47]. Furthermore, experiments comparing the tumor migration behavior of tumor antigen-experienced monocytes with unstimulated monocytes did not reveal any significant differences either. Nonetheless, a higher tendency of antigen-experienced

monocytes to accumulate in the liver-and-spleen was demonstrated over the first 4 days after systemic injection. Upon intratumoral injection of DiR-labelled monocytes, we could measure the DiR fluorescence for at least 3 weeks post injection without clear indications of leakage to the liver and/or the spleen. Over this period, a linear 3-fold decrease in DiR fluorescence was detected most probably due to degradation of the tracking dye rather than redistribution of labelled cells.

The similarities between monocyte and macrophage distributions suggest a tendency of systemically injected cells to accumulate in a non-specific manner. One can argue that that the similar distribution in the current study might in part be attributed to the lack of sufficient immunophenotypic differences between both populations. Indeed, even though the macrophages demonstrated a relatively more mature phenotypic profile based on the classical maturation markers ($F4/80^+/Ly6C^+/MHC\ II^+$), the injected macrophages still contained cells with a phenotypic profile of less mature monocytes. This heterogeneity is inherent to the used culture methods to generate macrophages or monocytes. Perhaps further separation of the monocytes and macrophages by a MACS-based negative selection protocol could have resulted in a more different migration pattern [48].

Our data corroborate the work of Ritchie et al. (2007) who reported that infused macrophage-activated killer (MAK) cells first accumulate in the liver, lungs and to a minor degree in the spleen, after which redistribution occurs from the pulmonary vasculature to other tissues including peritoneal metastases [49]. In line with this study and two other independent studies describing pulmonary redistribution of macrophages or MSCs, we also noticed a higher number of macrophages in the lungs 24 h after injection compared to 96 h after injection [5,36,49]. These kinetics may indicate that, also in our study, systemically injected macrophages are first partly sequestered in the lungs after which redistribution of these captured cells occurs to off-target organs such as the liver and the spleen as well as to on-target malignant sites. Supporting the current findings, Ritchie et al. (2007) described a much higher off-target versus on-target accumulation of these MAK cells as well. However, these authors report constant levels of MAK cells in liver and spleen, while the monocytes and macrophages in our study gradually declined in those organs. A possible explanation for this difference could be the difference in activation status upon injection i.e. their use of IFNγ-mediated macrophage activation as opposed to our use of unstimulated monocytes and macrophages.

To evaluate whether our immune cells actively migrate to tumors we subsequently inhibited the active migration capacity of macrophages by fixation. Surprisingly, the tumor migration of fixed macrophages did not differ from that of unfixed ones. This may indicate that the migration of the macrophages towards the tumors is a passive rather than an active process. Interestingly, fixed macrophages showed an increased retention in the lungs compared to their unfixed counterparts. Fixed macrophages have a lower capacity to deform and hence may cause a higher obstruction of the small lung vessels [50]. Despite the increased retention of the fixed macrophages in the lungs, no symptoms of pulmonary embolization were noticed.

The massive migration of injected monocytes and macrophages to the liver and spleen warranted to investigate whether some of the observed fluorescence could be attributed to labelling artefacts. DiR, a lipophilic NIR dye, integrates in cell membranes after short incubation with the cell suspension. As a result, dead cells or cell fragments originating from dead cells are also labelled with this dye and could partially mask the live cell-associated fluorescence. Therefore, the distribution of DiR-labelled dead cells/cell debris was assessed. As expected, this debris appeared to pass the lung capillary bed more easily than whole cells, but got captured—probably by the reticuloendothelial system—in the liver and spleen. Dead cells/cell fragments also accumulated in the tumors, although there was a non-significant trend of lower *in vivo* accumulation in the tumor than the live cells. These data illustrated that DiR labelling artefacts originating from labelled dead cells/cell fragments should not be ignored when considering the *in vivo* distribution of live cells. However, since only a limited number of dead cells/cell fragments (around 10%) were injected in our experiments, we only expect a minor impact on our migration data. Additionally, flow cytometry on single cell suspensions of the different tissues confirmed that viable DiR-labelled cells were present in the tumor, liver, spleen and lungs after intravenous injection of DiR-labelled macrophages. Another concern was the potential residual dye remaining in the supernatant of injected cell suspensions. Hypothetically, it could label cells *in vivo* (e.g. hematopoietic cells or endothelial cells). However, we demonstrated that residual free dye in the cell suspension did not increase the fluorescence in the tumor and tissues above background.

Besides MSCs, monocytes and macrophages, MDSCs have also been exploited in several studies for their superior tumor-homing properties [8,51-54]. Eisenstein et al. (2013) reported monocytic MDSCs to significantly outperform other leukocyte subsets such as naïve T cells or IL-2 activated T cells, monocytes, macrophages and dendritic cells as far as their tumor tropism to hepatic Lewis Lung Carcinoma (LLC) tumors is concerned [8]. In contrast, substantial *in vivo* differences in tumor tropism between MDSCs (either directly from bone marrow samples or after *in vitro* differentiation) and healthy bone marrow cells were not observed in our study. This striking difference might at least partly be explained by the considerable number of $CD11b^+Ly6G^+Ly6C^{int}$ granulocytic MDSCs (about 45%) compared to $CD11b^+Ly6G^-Ly6C^{hi}$ monocytic MDSCs (8-13%) present in our injected MDSCs. To our knowledge, no publications are available that directly compare the tumor tropism of granulocytic versus monocytic MDSCs. A second possibility is that the used MDSCs are less recruited to fat pad tumors compared to the intrahepatic tumor model as used by Eisenstein et al. (2013) [8]. Nevertheless, this latter argument seems unlikely since 4T1 tumors are known to generate a large number of MDSCs [30,31]. Lastly, since Eisenstein et al. used an intrahepatic LLC model, tumor-associated accumulation of monocytic MDSCs could partly overlap the liver-associated accumulation and hence, induce false positive results.

Overall, the use of cellular vehicles to deposit toxic agents in tumors after systemic administration requires these vehicles to specifically accumulate in the tumor. In the current study, relevant numbers of injected cells were found at the tumor location, but a substantial off-target migration was also seen in the liver, spleen and the lungs. Since the general trend of this off-target migration was declining over time whereas the tumor-associated accumulation remained constant or slowly increased, we plotted this relative shift. The steady accumulation in the tumor until the moment of euthanasia alludes to the existence of a peak at later timepoints. We therefore suggest that gene modified cellular vehicles that contain a genetic ON/OFF switch in the expression cassette of the therapeutic gene would allow to switch on the expression of toxic agents when the

relative percentage of on-target tumor accumulation is maximal [55]. This point could be determined by incorporation of reporter genes as longitudinal trackers [56]. Interestingly, the described 'relative on-target fraction' indicates that fresh bone marrow cells from either healthy or tumor-bearing donors have superior properties compared to cultured monocytes and macrophages. It is tempting to attribute this property to the relatively unmanipulated state of these cells, but since the *in vitro* differentiated MDSCs exhibited a similar profile, this explanation may not suffice. Based on our former findings [57], we aim to transfect primary myeloid cells with a gene coding for IL-12. Successful expression of this gene near solid tumors would not only stimulate cellular immunity against tumor antigens [58], but can also polarize myeloid cells toward an anti-tumoral phenotype [59,60].

We can conclude that the accumulation of immune cells in tumors mainly occurs via a non-specific passive process. Indeed, bone marrow cells from healthy or tumor-bearing donors, as well as *in vitro* differentiated MDSCs, monocytes or macrophages and fixated macrophages all demonstrate a comparable tumor-associated fluorescence upon intravenous injection. In addition, marked off-target sequestration of injected immune cells can be seen in the liver, spleen and the lungs. The relative on-target percentage calculation reveals that uncultured ('fresh') primary immune cells, followed by cultured MDSCs, had superior distribution profiles compared to cultured monocytes and macrophages. One way or another, the off-target migration of cellular vehicles intended for tumor targeted delivery should be addressed when pursuing true tumor-specific delivery.

## Declarations of interest

None.

## Funding

This work was supported by the Research Foundation -Flanders (FWO) (grant number 1119318N). Francis Combes is a fellow of the Research Foundation – Flanders (FWO). With support of the University Foundation of Belgium.

## Acknowledgements

The authors would like to thank prof. dr. Olivier De Wever for the use of the Miltenyi gentleMACS system.

## Appendix A. Supplementary data

Supplementary data to this article can be found online at https://doi.org/10.1016/j.neo.2018.06.005.

## References

[1] Harrington K, Alvarez-Vallina L, Crittenden M, Gough M, Chong H, Diaz RM, Vassaux G, Lemoine N, and Vile R (2002). Cells as vehicles for cancer gene therapy: the missing link between targeted vectors and systemic delivery? *Hum Gene Ther* **13**(11), 1263–1280.

[2] Medzhitov R (2008). Origin and physiological roles of inflammation. *Nature* **454** (7203), 428–435.

[3] Roth JC, Curiel DT, and Pereboeva L (2008). Cell vehicle targeting strategies. *Gene Ther* **15**(10), 716–729.

[4] Lim WA and June CH (2017). The principles of engineering immune cells to treat cancer. *Cell* **168**(4), 724–740.

[5] Choi YJ, Oh SG, Singh TD, Ha JH, Kim DW, Lee SW, Jeong SY, Ahn BC, Lee J, and Jeon YH (2016). Visualization of the biological behavior of tumor-associated macrophages in living mice with colon cancer using multimodal optical reporter gene imaging. *Neoplasia* **18**(3), 133–141.

[6] Suratt BT, Young SK, Lieber J, Nick JA, Henson PM, and Worthen GS (2001). Neutrophil maturation and activation determine anatomic site of clearance from circulation. *Am J Physiol Lung Cell Mol Physiol* **281**(4), L913–L921.

[7] De Becker A and Riet IV (2016). Homing and migration of mesenchymal stromal cells: How to improve the efficacy of cell therapy? *World J Stem Cells* **8**(3), 73–87.

[8] Eisenstein S, Coakley BA, Briley-Saebo K, Ma G, Chen HM, Meseck M, Ward S, Divino C, Woo S, and Chen SH, et al (2013). Myeloid-derived suppressor cells as a vehicle for tumor-specific oncolytic viral therapy. *Cancer Res* **73**(16), 5003–5015.

[9] Vinogradov S, Warren G, and Wei X (2014). Macrophages associated with tumors as potential targets and therapeutic intermediates. *Nanomedicine* **9**(5), 695–707.

[10] Zilio S and Serafini P (2016). Neutrophils and Granulocytic MDSC: The Janus God of Cancer Immunotherapy. *Vaccines* **4**(3).

[11] Shan L (2004). Near-infrared fluorescence 1,1-dioctadecyl-3,3,3,3-tetramethylindotricarbocyanine iodide (DiR)-labeled macrophages for Cell imaging. Molecular Imaging and Contrast Agent Database (MICAD). (US): Bethesda (MD): National Center for Biotechnology Information; 2004.

[12] Eisenblatter M, Ehrchen J, Varga G, Sunderkotter C, Heindel W, Roth J, Bremer C, and Wall A (2009). In vivo optical imaging of cellular inflammatory response in granuloma formation using fluorescence-labeled macrophages. *J Nucl Med* **50**(10), 1676–1682.

[13] Youniss FM, Sundaresan G, Graham LJ, Wang L, Berry CR, Dewkar GK, Jose P, Bear HD, and Zweit J (2014). Near-infrared imaging of adoptive immune cell therapy in breast cancer model using cell membrane labeling. *PLoS One* **9**(10) e109162.

[14] Du X, Wang X, Ning N, Xia S, Liu J, Liang W, Sun H, and Xu Y (2012). Dynamic tracing of immune cells in an orthotopic gastric carcinoma mouse model using near-infrared fluorescence live imaging. *Exp Ther Med* **4**(2), 221–225.

[15] Liu H and Wu D (2016). In vivo near-infrared fluorescence tumor imaging using DiR-loaded nanocarriers. *Curr Drug Deliv* **13**(1), 40–48.

[16] Amend SR, Valkenburg KC, and Pienta KJ (2016). Murine hind limb long bone dissection and bone marrow isolation. *J Vis Exp* (110).

[17] Su S, Zhao Q, He C, Huang D, Liu J, Chen F, Chen J, Liao JY, Cui X, and Zeng Y, et al (2015). miR-142-5p and miR-130a-3p are regulated by IL-4 and IL-13 and control profibrogenic macrophage program. *Nat Commun* **6**, 8523.

[18] Wagner M, Koester H, Deffge C, Weinert S, Lauf J, Francke A, Lee J, Braun-Dullaeus RC, and Herold J (2014). Isolation and intravenous injection of murine bone marrow derived monocytes. *J Vis Exp* (94).

[19] Liechtenstein T, Perez-Janices N, Gato M, Caliendo F, Kochan G, Blanco-Luquin I, Van der Jeught K, Arce F, Guerrero-Setas D, and Fernandez-Irigoyen J, et al (2014). A highly efficient tumor-infiltrating MDSC differentiation system for discovery of anti-neoplastic targets, which circumvents the need for tumor establishment in mice. *Oncotarget* **5**(17), 7843–7857.

[20] Dufait I, Schwarze JK, Liechtenstein T, Leonard W, Jiang H, Escors D, De Ridder M, and Breckpot K (2015). Ex vivo generation of myeloid-derived suppressor cells that model the tumor immunosuppressive environment in colorectal cancer. *Oncotarget* **6**(14), 12369–12382.

[21] Steel CD, Stephens AL, Hahto SM, Singletary SJ, and Ciavarra RP (2008). Comparison of the lateral tail vein and the retro-orbital venous sinus as routes of intravenous drug delivery in a transgenic mouse model. *Lab Anim* **37**(1), 26–32.

[22] Yardeni T, Eckhaus M, Morris HD, Huizing M, and Hoogstraten-Miller S (2011). Retro-orbital injections in mice. *Lab Anim* **40**(5), 155–160.

[23] Leon-Rico D, Fernandez-Garcia M, Aldea M, Sanchez R, Peces-Barba M, Martinez-Palacio J, Yanez RM, and Almarza E (2015). Comparison of haematopoietic stem cell engraftment through the retro-orbital venous sinus and the lateral vein: alternative routes for bone marrow transplantation in mice. *Lab Anim* **49**(2), 132–141.

[24] Nanni C, Pettinato C, Ambrosini V, Spinelli A, Trespidi S, Rubello D, Al-Nahhas A, Franchi R, Alavi A, and Fanti S (2007). Retro-orbital injection is an effective route for radiopharmaceutical administration in mice during small-animal PET studies. *Nucl Med Commun* **28**(7), 547–553.

[25] Andersen MN, Al-Karradi SN, Kragstrup TW, and Hokland M (2016). Elimination of erroneous results in flow cytometry caused by antibody binding to Fc receptors on human monocytes and macrophages. *Cytometry A* **89**(11), 1001–1009.

[26] Sun X, Gao D, Gao L, Zhang C, Yu X, Jia B, Wang F, and Liu Z (2015). Molecular imaging of tumor-infiltrating macrophages in a preclinical mouse model of breast cancer. *Theranostics* **5**(6), 597–608.

[27] Makela AV, Gaudet JM, and Foster PJ (2017). Quantifying tumor associated macrophages in breast cancer: a comparison of iron and fluorine-based MRI cell tracking. *Sci Rep* **7**, 42109.

[28] Safarzadeh E, Orangi M, Mohammadi H, Babaie F, and Baradaran B (2017). Myeloid-derived suppressor cells: important contributors to tumor progression and metastasis. *J Cell Physiol* **233**, 3024–3036.

[29] Hamilton MJ, Banath JP, Lam V, Lepard NE, Krystal G, and Bennewith KL (2012). Serum inhibits the immunosuppressive function of myeloid-derived suppressor cells isolated from 4T1 tumor-bearing mice. *Cancer Immunol Immunother* **61**(5), 643–654.

[30] Youn JI, Nagaraj S, Collazo M, and Gabrilovich DI (2008). Subsets of myeloid-derived suppressor cells in tumor-bearing mice. *J Immunol* **181**(8), 5791–5802.

[31] Donkor MK, Lahue E, Hoke TA, Shafer LR, Coskun U, Solheim JC, Gulen D, Bishay J, and Talmadge JE (2009). Mammary tumor heterogeneity in the expansion of myeloid-derived suppressor cells. *Int Immunopharmacol* **9**(7-8), 937–948.

[32] Danilin S, Merkel AR, Johnson JR, Johnson RW, Edwards JR, and Sterling JA (2012). Myeloid-derived suppressor cells expand during breast cancer progression and promote tumor-induced bone destruction. *Oncoimmunology* **1**(9), 1484–1494.

[33] Ouzounova M, Lee E, Piranlioglu R, El Andaloussi A, Kolhe R, Demirci MF, Marasco D, Asm I, Chadli A, and Hassan KA, et al (2017). Monocytic and granulocytic myeloid derived suppressor cells differentially regulate spatiotemporal tumour plasticity during metastatic cascade. *Nat Commun* **8**, 14979.

[34] Caplan AI and Sorrell JM (2015). The MSC curtain that stops the immune system. *Immunol Lett* **168**(2), 136–139.

[35] Devine SM, Cobbs C, Jennings M, Bartholomew A, and Hoffman R (2003). Mesenchymal stem cells distribute to a wide range of tissues following systemic infusion into nonhuman primates. *Blood* **101**(8), 2999–3001.

[36] Leibacher J and Henschler R (2016). Biodistribution, migration and homing of systemically applied mesenchymal stem/stromal cells. *Stem Cell Res Ther* **7**, 7.

[37] DuPre SA, Redelman D, and Hunter Jr KW (2007). The mouse mammary carcinoma 4T1: characterization of the cellular landscape of primary tumours and metastatic tumour foci. *Int J Exp Pathol* **88**(5), 351–360.

[38] duPre SA, Redelman D, and Hunter Jr KW (2008). Microenvironment of the murine mammary carcinoma 4T1: endogenous IFN-gamma affects tumor phenotype, growth, and metastasis. *Exp Mol Pathol* **85**(3), 174–188.

[39] Elpek KG, Cremasco V, Shen H, Harvey CJ, Wucherpfennig KW, Goldstein DR, Monach PA, and Turley SJ (2014). The tumor microenvironment shapes lineage, transcriptional, and functional diversity of infiltrating myeloid cells. *Cancer Immunol Res* **2**(7), 655–667.

[40] Panni RZ, Linehan DC, and DeNardo DG (2013). Targeting tumor-infiltrating macrophages to combat cancer. *Immunotherapy* **5**(10), 1075–1087.

[41] Kumar V, Patel S, Tcyganov E, and Gabrilovich DI (2016). The nature of myeloid-derived suppressor cells in the tumor microenvironment. *Trends Immunol* **37**(3), 208–220.

[42] Ueha S, Shand FH, and Matsushima K (2011). Myeloid cell population dynamics in healthy and tumor-bearing mice. *Int Immunopharmacol* **11**(7), 783–788.

[43] Gerhardt T and Ley K (2015). Monocyte trafficking across the vessel wall. *Cardiovasc Res* **107**(3), 321–330.

[44] van Furth R and Cohn ZA (1968). The origin and kinetics of mononuclear phagocytes. *J Exp Med* **128**(3), 415–435.

[45] Hume DA, Robinson AP, MacPherson GG, and Gordon S (1983). The mononuclear phagocyte system of the mouse defined by immunohistochemical localization of antigen F4/80. Relationship between macrophages, Langerhans cells, reticular cells, and dendritic cells in lymphoid and hematopoietic organs. *J Exp Med* **158**(5), 1522–1536.

[46] Yang J, Zhang L, Yu C, Yang XF, and Wang H (2014). Monocyte and macrophage differentiation: circulation inflammatory monocyte as biomarker for inflammatory diseases. *Biomark Res* **2**(1), 1.

[47] Sunderkotter C, Nikolic T, Dillon MJ, Van Rooijen N, Stehling M, Drevets DA, and Leenen PJ (2004). Subpopulations of mouse blood monocytes differ in maturation stage and inflammatory response. *J Immunol* **172**(7), 4410–4417.

[48] Oliva-Martin MJ, Sanchez-Abarca LI, Carrillo-Jimenez A, Perez-Simon JA, and Venero JL (2015). Evaluation of a method for murine monocyte isolation by bone marrow depletion. *Anal Biochem* **480**, 42–48.

[49] Ritchie D, Mileshkin L, Wall D, Bartholeyns J, Thompson M, Coverdale J, Lau E, Wong J, Eu P, and Hicks RJ, et al (2007). In vivo tracking of macrophage activated killer cells to sites of metastatic ovarian carcinoma. *Cancer Immunol Immunother* **56**(2), 155–163.

[50] Melder RJ, Kristensen CA, Munn LL, and Jain RK (2001). Modulation of A-NK cell rigidity: In vitro characterization and in vivo implications for cell delivery. *Biorheology* **38**(2-3), 151–159.

[51] Chandra D and Gravekamp C (2013). Myeloid-derived suppressor cells: cellular missiles to target tumors. *Oncoimmunology* **2**(11)e26967.

[52] Quispe-Tintaya W, Chandra D, Jahangir A, Harris M, Casadevall A, Dadachova E, and Gravekamp C (2013). Nontoxic radioactive Listeria(at) is a highly effective therapy against metastatic pancreatic cancer. *Proc Natl Acad Sci U S A* **110**(21), 8668–8673.

[53] Pan PY, Chen HM, and Chen SH (2013). Myeloid-derived suppressor cells as a Trojan horse: A cellular vehicle for the delivery of oncolytic viruses. *Oncoimmunology* **2**(8)e25083.

[54] Chandra D, Jahangir A, Quispe-Tintaya W, Einstein MH, and Gravekamp C (2013). Myeloid-derived suppressor cells have a central role in attenuated Listeria monocytogenes-based immunotherapy against metastatic breast cancer in young and old mice. *Br J Cancer* **108**(11), 2281–2290.

[55] Weber W and Fussenegger M (2011). Molecular diversity–the toolbox for synthetic gene switches and networks. *Curr Opin Chem Biol* **15**(3), 414–420.

[56] Kim JE, Kalimuthu S, and Ahn BC (2015). In vivo cell tracking with bioluminescence imaging. *Nucl Med Mol Imaging* **49**(1), 3–10.

[57] Denies S, Combes F, Ghekiere C, Mc Cafferty S, Cicchelero L, and Sanders NN (2017). In vitro exploration of a myeloid-derived suppressor cell line as vehicle for cancer gene therapy. *Cancer Gene Ther* **24**(4), 149–155.

[58] Del Vecchio M, Bajetta E, Canova S, Lotze MT, Wesa A, Parmiani G, and Anichini A (2007). Interleukin-12: biological properties and clinical application. *Clin Cancer Res* **13**(16), 4677–4685.

[59] Steding CE, Wu ST, Zhang Y, Jeng MH, Elzey BD, and Kao C (2011). The role of interleukin-12 on modulating myeloid-derived suppressor cells, increasing overall survival and reducing metastasis. *Immunology* **133**(2), 221–238.

[60] Yu XL, Wu BT, Ma TT, Lin Y, Cheng F, Xiong HY, Xie CL, Liu CY, Wang Q, and Li ZW, et al (2016). Overexpression of IL-12 reverses the phenotype and function of M2 macrophages to M1 macrophages. *Int J Clin Exp Pathol* **9**(9), 8963–8972.